JOURNAL OF MATERIALS SCIENCE 25 (1990) 4080–4086

Effects of interfacial bonding on sliding phenomena during compressive loading of an embedded fibre

CHUN-HWAY HSUEH
Metals and Ceramics Division, Oak Ridge National Laboratory, Oak Ridge, Tennessee 37831, USA

The effects of interfacial bonding on the sliding phenomena at the fibre/matrix interface are considered for fibre-reinforced ceramic composites when an axial compressive stress is applied at the exposed end of an embedded fibre. Sliding occurs at the interface when the interfacial shear strength is exceeded. The interfacial shear stress, the stress transfer from the fibre to the matrix, the length of the sliding zone, and the fibre displacement are analysed in the present study. The results show that at a fixed load, the sliding length and the fibre displacement decrease with increase in the interfacial shear strength. Effects of interfacial bonding on the applied stress–fibre displacement relationship during compressive loading and subsequent unloading are also revealed.

1. Introduction

The properties at the fibre/matrix interface influence the mechanical behaviour of fibre-reinforced ceramic composites. One of the most significant toughening mechanisms in such composites is the bridging of the crack surfaces by intact fibres when the composite is subjected to tension. While the bridging stresses in fibres contribute to the toughening effect, relative displacement in the loading direction between fibres and the matrix at the crack surface is required to accommodate the crack opening displacement. Consequently, optimal conditions for toughening of these composites require debonding at fibre/matrix interfaces by shear during fibre pullout, and allow frictional sliding between fibres and the matrix [1–3]. These requirements have prompted studies of interfacial properties of composites: the interfacial shear strength associated with debonding and, after debonding, the interfacial frictional stress [4–14].

The effects of the coefficient of friction, the residual clamping stress at the interface, and the elastic constants of the constituent materials on the interfacial sliding phenomena of composites have been analysed theoretically for an embedded fibre subjected to an applied stress at its exposed end along its axial direction [12–14]. However, those results are based on the condition of an unbonded and frictional interface, which maximizes the toughening effect. In general, chemical or mechanical bonding is often unavoidable at the interface during processing of the composite [14]. As a complement of previous studies [12–14], the effects of interfacial bonding on the sliding phenomena are considered in the present work. First, the solution of the fibre displacement is given when the interface is bonded, and the condition for interfacial debonding is addressed. Then, when the interface is partially debonded, the interfacial shear stress, the stress transfer from the fibre to the matrix, the length of the sliding zone, and the fibre displacement are analysed. Finally, the effects of interfacial bonding on the applied stress–fibre displacement relationship during compressive loading and subsequent unloading are shown.

2. Analyses

The geometry of the system considered in the present study is a composite cylinder model [15], which is also used in previous studies [12–14]. A semi-infinitely long fibre with a radius, a , is located at the centre of a coaxial cylindrical shell of the matrix with an outer radius, b. A bonded fibre/matrix interface is considered in the present analysis. As shown in Fig. 1, z is the direction parallel to the fibre axis and r is the radial distance from the fibre axis. An axial compressive stress, σ_0 (negative for compression), is applied at the exposed end of the embedded fibre (i.e. at $z = l$ in Fig. 1). For convenience, when comparing compressive stresses, the negative sign is omitted and only the magnitude is implied in the text. When the applied axial compressive stress is lower than that of a critical compressive stress, σ_d, the bonded interface remains intact (Fig. 1a). However, when the applied axial stress exceeds this critical stress, debonding and sliding are initiated at the surface and extend to a depth l beneath the surface, such that the end of the sliding zone located at $z = 0$ (Fig. 1b).

2.1. Bonded interface

The problem of the elastic stress transfer from an embedded fibre to the surrounding matrix for the case of a bonded interface has been analysed [3]. When the fibre is subjected to an axial compressive stress (σ_0) at

0022–2461/90 $03.00 + .12

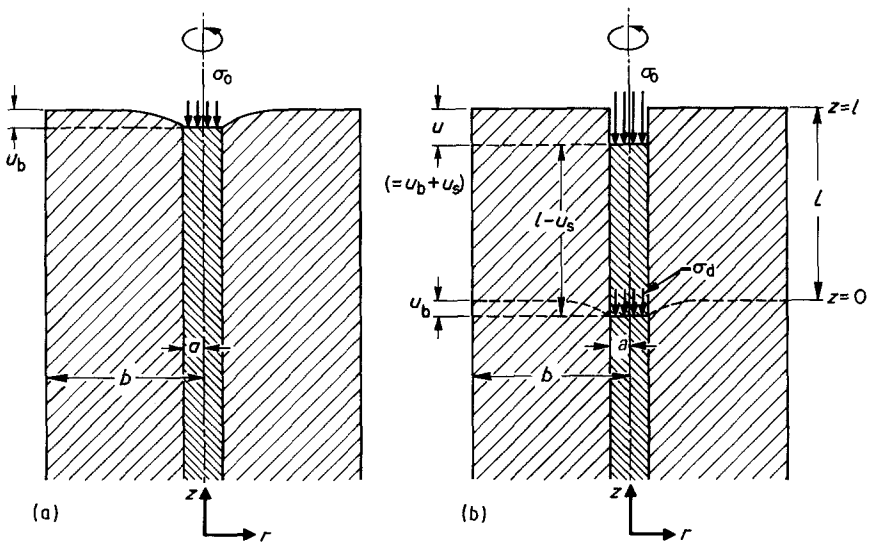

Figure 1 Schematic illustration of the composite cylinder model for (a) a bonded interface when the applied compressive stress is low ($|\sigma_0| \leqslant |\sigma_d|$), and (b) debonding and sliding when $|\sigma_0| > |\sigma_d|$, also showing the fibre displacement.

its exposed end, the stress is transferred from the fibre to the matrix through the interfacial shear stress. Relative displacement between the fibre and the matrix is prohibited at the interface when the interface is bonded. However, a relative displacement exists between the fibre and the bulk of the matrix far from the interface. The maximum relative displacement, u_b, occurs at the surface (see Fig. 1a) and is related to the applied axial stress, σ_0, by [3]

$$u_b = \frac{a(b^2 - a^2)E_m\sigma_0}{a^2E_f + (b^2 - a^2)E_m} \times \left\{\frac{(1 + \nu_m)[a^2 - b^2 + b^2 \ln (b^2/a^2)]}{2E_f[a^2E_f + (b^2 - a^2)E_m]}\right\}^{1/2} \quad (1)$$

where E and ν are Young's modulus and Poisson's ratio, respectively, and the subscripts f and m denote the fibre and the matrix, respectively. The interfacial shear stress has a maximum value at the surface ($z = l$). Debonding is expected to initiate at the surface when the axially applied stress, σ_0, reaches a critical value, σ_d, for which the corresponding maximum interfacial shear stress reaches the interfacial shear strength, τ_s. The interfacial shear strength, τ_s, can then be related to σ_d by [3]

$$\tau_s = -(b^2 - a^2)E_m\sigma_d\{2E_f(1 + \nu_m) \times [a^2E_f + (b^2 - a^2)E_m] \times [a^2 - b^2 + b^2 \ln (b^2/a^2)]\}^{-1/2} \quad (2)$$

2.2. Interfacial debonding and sliding

When the interfacial shear strength is exceeded, debonding and frictional sliding occur at the interface. The solutions of fibre push-down subject to a residual clamping stress, σ_c, at the interface and an axial push-down stress, σ_0, have been derived for an unbonded interface [12]. In the presence of interfacial bonding, the boundary condition at the end of sliding needs to be modified as compared to the unbonded case. Without repeating the calculational procedures [12], the present paper gives only the differences required in deriving the solutions for the bonded case.

The equation governing the axial stress distribution in the fibre, σ_f, along the sliding length has been derived previously [12], such that

$$\sigma_f = \frac{A_3}{A_2} + X_1 \exp (m_1 z) + X_2 \exp (m_2 z) \quad (3)$$

where the coefficients, A_2, A_3, m_1 and m_2 are given by

$$A_2 = \frac{2\left[\left(1 - \frac{b^2}{a^2}\right)\frac{E_m\nu_f}{E_f\nu_m} - 1\right]}{(1 + \nu_m)[a^2 - b^2 + b^2 \ln (b^2/a^2)]} \quad (4)$$

$$A_3 = 2\left\{\sigma_0 + \left(1 - \frac{b^2}{a^2}\right)\left[1 + \frac{b^2 + a^2}{(b^2 - a^2)\nu_m} + \frac{E_m(1 - \nu_f)}{E_f\nu_m}\right]\sigma_c\right\} \times (1 + \nu_m)[a^2 - b^2 + b^2 \ln (b^2/a^2)] \quad (5)$$

$$m_1 = [-A_1 + (A_1^2 - 4A_2)^{1/2}]/2 \quad (6)$$

$$m_2 = [-A_1 - (A_1^2 - 4A_2)^{1/2}]/2 \quad (7)$$

and A_1 is given by

$$A_1 = \frac{a\left(1 - \frac{b^2}{a^2}\right)\left[1 + \frac{b^2 + a^2}{(b^2 - a^2)\nu_m} + \frac{E_m(1 - \nu_f)}{E_f\nu_m}\right]}{\mu(1 + \nu_m)[a^2 - b^2 + b^2 \ln (b^2/a^2)]} \quad (8)$$

where μ is the coefficient of friction at the sliding interface. The coefficients, X_1 and X_2, in Equation 3 can be determined from the following boundary conditions

$$\sigma_f = \sigma_0 \quad (\text{at } z = l) \quad (9)$$

$$\sigma_f = \sigma_d \quad (\text{at } z = 0) \quad (10)$$

Equations 9 and 10 dictate that axial stresses in the fibre are in equilibrium with the applied stress and the bonding strength at the loaded surface and the end of sliding, respectively. Solution of σ_f (Equation 3) subject to the boundary conditions given by Equations 9 and 10, yields

$$X_1 = \frac{\sigma_0 - \sigma_d \exp (m_2 l) - (A_3/A_2)[1 - \exp (m_2 l)]}{\exp (m_1 l) - \exp (m_2 l)} \quad (11)$$

$$X_2 = \sigma_d - \frac{A_3}{A_2} - X_1 \quad (12)$$

The corresponding interfacial shear stress (τ_i), the interfacial radial stress (σ_r), the axial stress in the matrix at the interface (σ_a), and the axial displacement in the fibre (w_f) due to sliding are [12]

$$\tau_i = -\frac{a}{2}\left\{-\frac{m_2 A_3 \exp(m_2 z)}{A_2} + X_1[m_1 \exp(m_1 z) - m_2 \exp(m_2 z)] + \sigma_d m_2 \exp(m_2 z)\right\} \quad (13)$$

$$\sigma_r = \frac{\tau_i}{\mu} - \sigma_c \quad (14)$$

$$\sigma_a = -\left[1 + \frac{b^2 + a^2}{(b^2 - a^2)\nu_m} + \frac{E_m(1 - \nu_f)}{E_f \nu_m}\right]\sigma_r + \frac{E_m \nu_f \sigma_f}{E_f \nu_m} \quad (15)$$

$$w_f = \frac{1}{E_f}\left\{\frac{A_3 z}{A_2} + \frac{A_3[1 - \exp(m_2 z)]}{m_2 A_2} + X_1\left[\frac{\exp(m_1 z) - 1}{m_1} - \frac{\exp(m_2 z) - 1}{m_2}\right] + \frac{\sigma_d[\exp(m_2 z) - 1]}{m_2}\right\} \quad (16)$$

The axial displacement in the fibre due to sliding, w_f, has a maximum value, u_s, at the surface (see Fig. 1b). Solutions of the interfacial properties given by Equations 3, 13 to 16 are contingent upon the solution of the length of the sliding zone, l, which can be determined from the continuity condition at the end of the sliding zone.

At the end of sliding, the relative displacement between the fibre and the matrix at the interface is prohibited. This condition requires continuity of the axial strains of the fibre and the matrix at the end of sliding, such that [12]

$$\frac{1}{E_f}[\sigma_d - 2\nu_f \sigma_r] = \frac{1}{E_m}\left[\sigma_a + \frac{2a^2 \nu_m \sigma_r}{b^2 - a^2}\right] \quad (\text{at } z = 0) \quad (17)$$

Substitutions of σ_r and σ_a given by Equations 14 and 15 in Equation 17 yields the relationship between the length of the sliding zone, l, and the axial stress required for debonding, σ_d, such that

$$\left[2\left(\frac{a^2 \nu_m}{b^2 - a^2} + \frac{E_m \nu_f}{E_f}\right) - 1 - \frac{b^2 + a^2}{(b^2 - a^2)\nu_m} - \frac{E_m(1 - \nu_f)}{E_f \nu_m}\right] \times \left\{\frac{a}{2\mu}\left[\frac{m_2 A_3}{A_2} - \frac{(m_1 - m_2)[\sigma_0 - (A_3/A_2)[1 - \exp(m_2 l)]]}{\exp(m_1 l) - \exp(m_2 l)}\right] - \sigma_c\right\} = \left\{\frac{E_m}{E_f}\left(1 - \frac{\nu_f}{\nu_m}\right) + \frac{a}{2\mu}\left[2\left(\frac{a^2 \nu_m}{b^2 - a^2} + \frac{E_m \nu_f}{E_f}\right) - 1 - \frac{b^2 + a^2}{(b^2 - a^2)\nu_m} - \frac{E_m(1 - \nu_f)}{E_f \nu_m}\right] \times \left[m_2 - \frac{(m_1 - m_2)\exp(m_2 l)}{\exp(m_1 l) - \exp(m_2 l)}\right]\right\}\sigma_d \quad (18)$$

Hence, with a given value of the interfacial shear strength, τ_s, the corresponding axial stress in the fibre required to initiate debonding, σ_d, can be obtained from Equation 2. With σ_d obtained, the length of the sliding zone, l, can be derived from Equation 18. With the solution of l, the descriptions of the interfacial properties (Equations 3, 13 to 16) are complete.

3. Results

Specific results are computed using the material properties of SiC fibre-reinforced Al_2O_3 with $E_f = 500$ GPa, $E_m = 400$ GPa, $\nu_f = 0.3$, and $\nu_m = 0.25$. The system, was also chosen previously [12–14]. Also, $b/a = 10$ (the results are not sensitive to b/a when $b/a \geqslant 10$), $\sigma_c/\sigma_0 = 0.1$ and $\mu = 0.1$ are used in the present calculation to elucidate the essential trends. Effects of interfacial bonding on sliding phenomena are shown by assuming arbitrarily the ratio of the interfacial shear strength to the applied axial stress, τ_s/σ_0.

3.1. Conditions for bonding and debonding

The ratio, τ_s/σ_0, is an important parameter in determining the bonding and the debonding conditions. With a fixed interfacial shear strength, τ_s, for a composite, the corresponding axial stress required to initiate debonding, σ_d, can be obtained from Equation 2. When the applied stress is higher than the value of σ_d, interfacial debonding and sliding occur. Otherwise, the interface remains intact. Modifications of the material properties to control the τ_s–σ_d relationship, and hence the fracture mechanism of the composite, have been addressed in a separate paper [3].

The normalized fibre displacement component due to the bonded interface, $u_b/a\sigma_0$ (where σ_0 is expressed in GPa), and the normalized axial stress in the fibre at the end of sliding, σ_d/σ_0, as functions of the normalized interfacial shear strength, $-\tau_s/\sigma_0$, are shown in Fig. 2. For the chosen materials properties (i.e. SiC–Al_2O_3), as the ratio of $-\tau_s/\sigma_0$ increases and reaches 0.29 (see Equation 2), the corresponding stress required for debonding, σ_d, increases and reaches the applied axial stress, σ_0. Hence, when $-\tau_s/\sigma_0 \geqslant 0.29$, the interface remains intact and the fibre displacement, u_b, is linearly proportional to the applied stress. However, when $-\tau_s/\sigma_0 < 0.29$, debonding and sliding occur such that both σ_d and u_b are linearly proportional to τ_s (see Fig. 2).

3.2. Effects of interfacial shear strength on sliding phenomena

The length of the sliding zone as a function of the

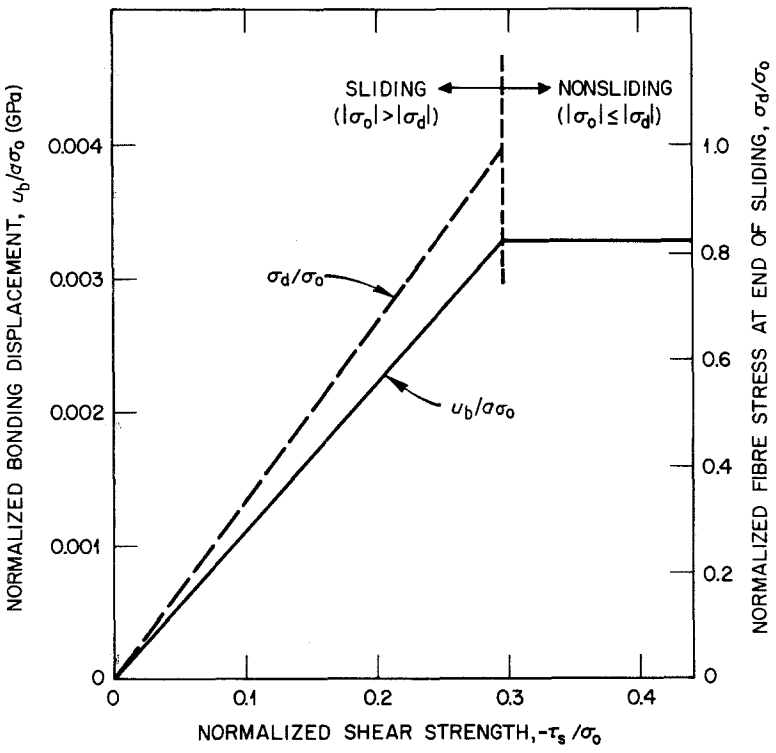

Figure 2 Normalized fibre displacement due to a bonded interface, $u_b/a\sigma_0$, and normalized axial stress in the fibre at the end of sliding, σ_d/σ_0, as functions of normalized interfacial shear strength, $-\tau_s/\sigma_0$, for $\sigma_c/\sigma_0 = 0.1$ and $\mu = 0.1$.

interfacial shear strength is shown in Fig. 3. At a fixed applied axial stress, the sliding length decreases with an increase in the interfacial shear strength. Effects of the interfacial shear strength on the axial stress distribution in the fibre and the interfacial shear stress along the sliding length, obtained from Equations 3 and 13, are shown in Figs 4a and b, respectively. The stress distributions within the sliding length are not sensitive to τ_s. However, the sliding length decreases with an increase in τ_s. The axial stress in the fibre is the applied axial stress at the loaded surface and decreases with the distance beneath the surface because of the stress transfer. Also, the interfacial shear stress is not constant along the sliding length because of Poisson's effect, which has been discussed in previous studies [12-14].

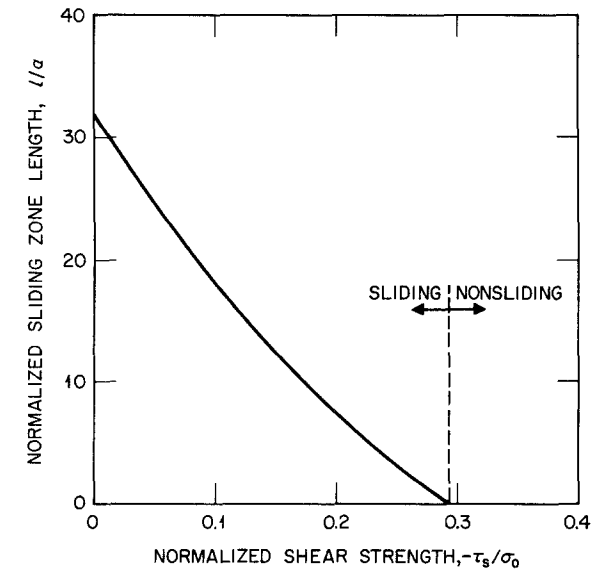

Figure 3 Normalized length of the sliding zone, l/a, as a function of normalized interfacial shear strength, $-\tau_s/\sigma_0$, for $\sigma_c/\sigma_0 = 0.1$ and $\mu = 0.1$.

For a bonded interface, the relationship between the fibre displacement and the applied axial stress is given by Equation 1 (also see Fig. 1a). When debonding and sliding occur, the total fibre displacement, u, consists of two components (see Fig. 1b): (1) the displacement, u_b, due to the bonded interface which is induced by the stress at the end of sliding (i.e. σ_d at $z = 0$), and (2) the displacement, u_s, due to relative sliding between the fibre and the matrix. The normalized fibre displacements are shown in Fig. 5 as functions of the normalized interfacial shear strength. The fibre displacement due to the bonded interface, u_b, was discussed in Section 2.1. At a fixed load, the fibre displacement due to sliding, u_s, decreases with an increase in τ_s, and is zero when sliding is prohibited (i.e. when $\tau_s/\sigma_0 > 0.29$ in Fig. 5). The resultant fibre displacement, u ($= u_b + u_s$), decreases with an increase in τ_s (see Fig. 5).

3.3. Effects of the interfacial shear strength on axial loading and unloading

The stress–fibre displacement relationship during axial compressive loading and subsequent unloading has been derived for the case of an unbonded interface [14]. Those results show that in the absence of Poisson's effect (i.e. $v_f = 0$), the loading curve is parabolic, and after complete unloading, the residual fibre displacement equals half of the fibre displacement at the peak load [5, 14]. When Poisson's effect increases (i.e. when v_f increases or the ratio of σ_c/σ^* decreases, where σ^* is the peak load), the loading curve shows a transition from parabolic to linear behaviour, and the ratio of the fibre displacement at complete unloading to that at peak loading (i.e. u_0/u^* in Fig. 6a) decreases from 0.5 to lower values [14]. A method for evaluating the coefficient of friction and the residual clamping stress from the loading and the unloading curves has also been demonstrated [14].

Effects of the interfacial shear strength on the load-

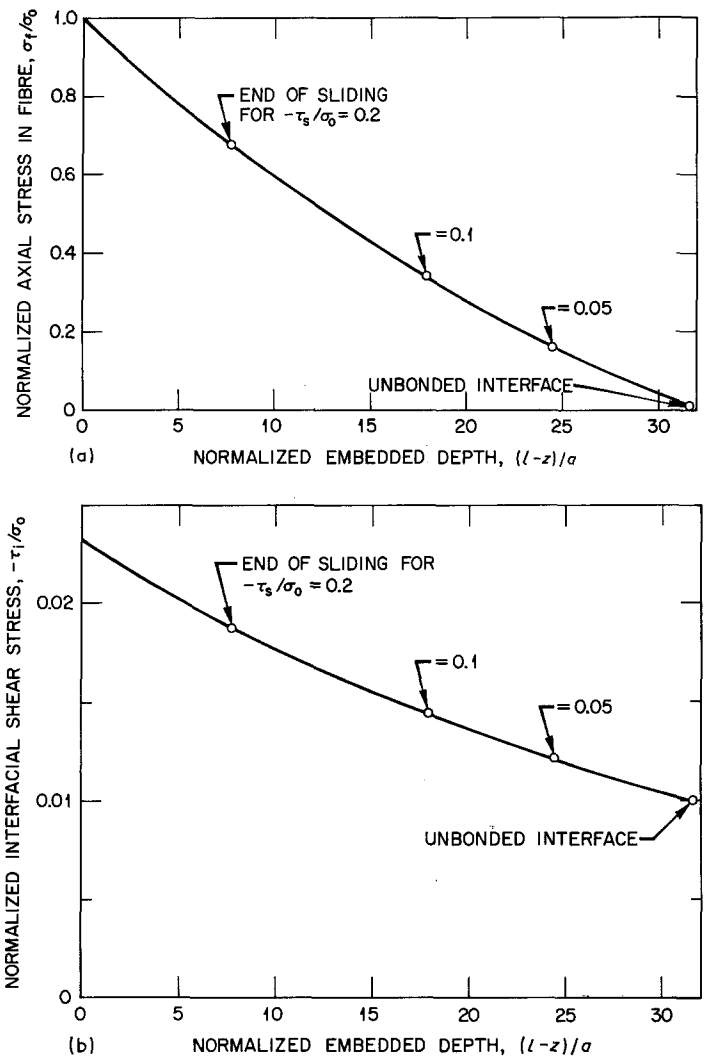

Figure 4 (a) Normalized axial stress in the fibre, σ_f/σ_0, and (b) normalized interfacial shear stress, $-\tau_i/\sigma_0$, along the sliding length, also showing the depth corresponding to the end of sliding for different ratios of $-\tau_s/\sigma_0$.

ing and the unloading curves are shown in Fig. 6a for $\sigma_c/\sigma^* = 0.1$, $\mu = 0.1$ and $-\tau_s/\sigma^* = 0.05$. For a bonded interface, when the applied compressive stress is lower than σ_d, the interface remains intact and the σ_0–u relationship is linear. As the compressive stress increases and exceeds σ_d, interfacial debonding and forward sliding of the fibre occur and the solutions are given by Equations 3, 13 to 16. During unloading, reverse sliding of the fibre occurs beginning at the surface and extending along the interface beneath the surface. However, the length of the reverse sliding zone at complete unloading is always less than the length of the forward sliding zone at peak loading [14]. Hence, even if the interface is bonded initially, reverse sliding occurs within the zone of the debonded interface resulting from the peak loading stress, σ^*, prior to unloading. The solutions derived in the previous study for unloading of an embedded fibre with an unbonded interface [14] remain valid for the case of an initially bonded interface.

Compared to the case of an unbonded interface, the loading curve shows an initial linear relationship with a lower compliance for the bonded case. Also, after complete unloading, the u_0/u^* ratio has a lower value

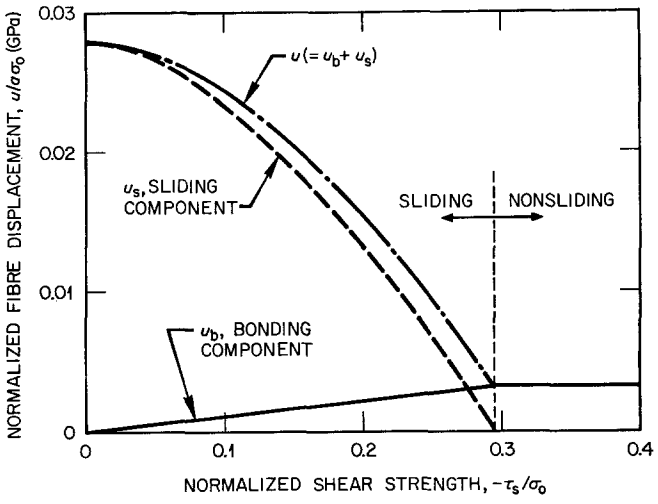

Figure 5 Normalized fibre displacement as a function of normalized interfacial shear strength for $\sigma_c/\sigma_0 = 0.1$ and $\mu = 0.1$.

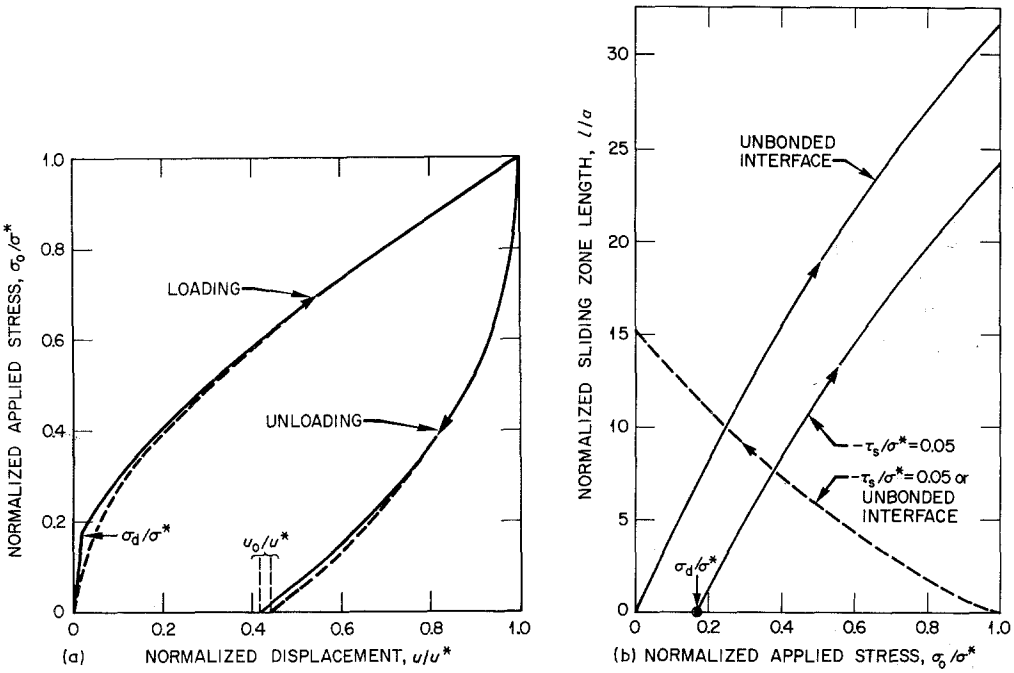

Figure 6 Effects of the interfacial shear strength on (a) the loading and the unloading curves, and (b) the lengths of the forward and the reverse sliding zones when (——) $-\tau_s/\sigma^* = 0.05$, $\sigma_c/\sigma^* = 0.1$ and $\mu = 0.1$. (– – –) Unbonded interface.

for the bonded case. Effects of the interfacial shear strength on sliding lengths are shown in Fig. 6b for $\sigma_c/\sigma^* = 0.1$, $\mu = 0.1$ and $-\tau_s/\sigma^* = 0.05$. For the bonded interface, a minimum stress, σ_d, is required to initiate forward sliding and the length of the forward sliding zone is shorter compared to the case of an unbonded interface. However, the length of the reverse sliding zone is the same for both the bonded and the unbonded interfaces (see Fig. 6b) because of the reason stated earlier.

3.4. Applications

It is noted that adoption of the composite cylinder model for the present analysis requires low volume fractions of fibres (e.g. $a^2/b^2 \leqslant 0.01$). In the presence of high volume fractions of fibres, the self-consistent model should be applied where the fibre is surrounded by a material, which has the properties of the composite [16]. The stress–displacement relationship of the fibre for Nicalon fibre-reinforced lithium aluminosilicate glass-ceramic was obtained by using the indentation technique (see Fig. 7) [5]. The properties of the materials are: $E_f = 200\,\text{GPa}$, $E_m = 80\,\text{GPa}$, $\nu_f = 0.15$ and $\nu_m = 0.3$ and the volume fraction of fibres is 0.3. Owing to the high volume fraction of fibres, the self consistent model is adopted, and the rule of mixtures is used to derive elastic constants of the composite to replace E_m and ν_m in the present analysis (i.e. E_m and ν_m become 116 GPa and 0.255, respectively). Comparison between the theoretical prediction and the experimental results shows that good agreement is obtained when $\sigma_d = -78\,\text{MPa}$, $\sigma_c = -21.5\,\text{MPa}$ and $\mu = 0.09$ are used in the theoretical prediction (see Fig. 7).

4. Discussion

The effects of interfacial bonding on the interfacial sliding phenomena of fibre-reinforced ceramic composites are shown in the present study. A simple interfacial debonding criterion is adopted by considering that debonding occurs when the maximum interfacial shear stress exceeds the interfacial shear strength, τ_s [4]. The residual clamping stress is not considered in deriving the stress required to initiate debonding, σ_d, for which the corresponding maximum interfacial shear stress reaches τ_s [3]. Further studies are required to establish pertinent debonding criteria. In the case of a multiaxial interfacial debonding criterion, the effect of the residual clamping stress on the interfacial shear strength should be included.

Experiments of axial compressive loading and subsequent unloading performed on Nicalon fibre-reinforced glass show the evidence of the interfacial bonding. At initial loading, displacement of the fibre in the loading direction indicates a higher resistance to movement (i.e. lower compliance). Then, when the loading stress exceeds a critical value, the loading curve shows a higher compliance. The experimental loading/unloading curves [5] are in good agreement

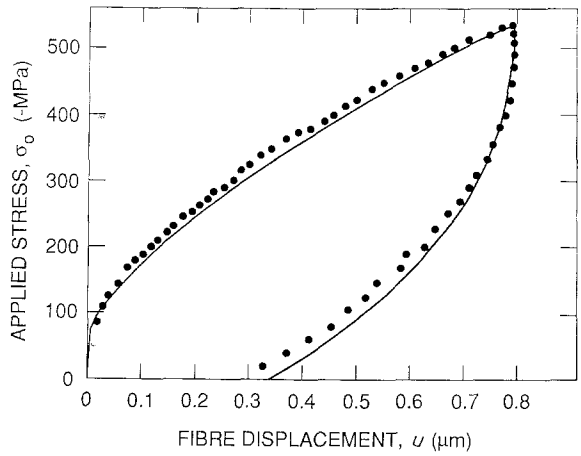

Figure 7 (●) Experimental data [5] and (——) the present prediction of the stress–displacement relationship during compressive loading and unloading for Nicalon-glass. $\sigma_d = -78\,\text{MPa}$, $\sigma_c = -21.5\,\text{MPa}$, $\mu = 0.09$.

with the prediction in the present study for the bonded interface. Modifications of the present analysis to consider the fibre pull-out test are addressed in a separate paper [17].

Finally, it is noted that crack "pop-in" during initiation of debonding, and the residual stress in the axial direction due to interfacial bonding are not considered in the present study. In the presence of crack pop-in, the stress–displacement relationship in Fig. 6a exhibits a discontinuity when the applied stress reaches σ_d and debonding initiates. In the presence of the residual axial stress, this residual stress should be superimposed on the applied stress as the resultant axial stress.

Acknowledgements

The author thanks Drs P. F. Becher, A. Bleier, and M. G. Jenkins for reviewing the manuscript. The research was sponsored by the Division of Materials Sciences, Office of Basic Energy Sciences, US Department of Energy, under contract DE-AC05-84OR21400 with Martin Marietta Energy Systems, Inc.

References

1. A. G. EVANS and R. M. McMEEKING, *Acta Metall.* **34** (1986) 2435.
2. P. F. BECHER, C. H. HSUEH, P. ANGELINI and T. N. TIEGS, *J. Amer. Ceram. Soc.* **12** (1988) 1050.
3. C. H. HSUEH and P. F. BECHER, *ibid.* submitted.
4. D. H. GRANDE, J. F. MANDELL and K. C. C. HONG, *J. Mater. Sci.* **23** (1988) 311.
5. D. B. MARSHALL and W. C. OLIVER, *J. Amer. Ceram. Soc.* **70** (1987) 542.
6. T. P. WEIHS, C. M. DICK and W. D. NIX, *Mater. Res. Soc. Symp. Proc.* **120** (1988) 247.
7. R. N. SINGH, *ibid.* **120** (1988) 259.
8. D. K. SHETTY, *J. Amer. Ceram. Soc.* **71** (1988) C107.
9. K. T. FABER, S. H. ADVANI, J. K. LEE and J. T. JINN, *ibid.* **69** (1986) C208.
10. C. H. HSUEH, *ibid.* **71** (1988) 490.
11. *Idem, J. Mater. Sci. Lett.* **8** (1989) 739.
12. *Idem, J. Mater. Sci.*, **25** (1990) 818.
13. *Idem, ibid.* **25** (1990) 811.
14. C. H. HSUEH, M. K. FERBER and P. F. BECHER, *J. Mater. Res.*, **4** (1989) 1529.
15. Z. HASHIN and B. W. ROSEN, *J. Appl. Mech.* **31** (1964) 223.
16. Z. HASHIN and S. SHTRIKMAN, *J. Mech. Phys. Solids* **11** (1963) 127.
17. C. H. HSUEH, *Acta Metall.*, **38** (1990) 403.

Received 27 April
and accepted 29 November 1989